IEEE Access
Multidisciplinary | Rapid Review | Open Access Journal

Received March 16, 2020, accepted April 6, 2020, date of publication April 14, 2020, date of current version April 30, 2020.

Digital Object Identifier 10.1109/ACCESS.2020.2987651

Study on Composite Electromagnetic Scattering Characteristics of Low-Altitude Target Above Valley Composite Rough Surface Using Hybrid SBR-EEC Method

GAOXIANG ZOU[1], CHUANGMING TONG[1], JIAN ZHU[2], HUALONG SUN[1], AND PENG PENG[1]

[1]Air Force Engineering University, Xi'an 710051, China
[2]Shanghai Radio Equipment Research Institute, Shanghai 200090, China

Corresponding author: Gaoxiang Zou (gxiangzou@163.com)

This work was supported by the National Natural Science Foundations of China under Grant 61372033 and Grant 61901510.

ABSTRACT The composite electromagnetic (EM) scattering characteristics of low-altitude target above valley composite rough surface are studied. The composite rough surface modeling theory is adopted to simulate the natural cavity structure of valley environment. Aiming at efficiently and accurately calculate the composite EM scattering from low-altitude target above valley environment, a hybrid method combining shooting and bouncing ray (SBR) technique and equivalent edge currents (EEC) method is proposed, in which SBR method based on the ray-density normalization (RDN) is applied to consider the multiple interactions between target and environment, and EEC method meliorates target's edge diffraction. Numerical examples illustrate the efficiency and validation of proposed hybrid method. Finally, based on the hybrid SBR-EEC method, the EM scattering characteristics of low-altitude target above valley environment are further investigated to show scattering mechanisms of this composite model and provide some useful conclusions through physical phenomena.

INDEX TERMS Valley composite rough surface, shooting and bouncing ray technique, equivalent edge currents method, composite electromagnetic scattering.

I. INTRODUCTION

In recent years, study on electromagnetic (EM) scattering characteristic of target with cavity structure has been a concerned focus in computational electromagnetism. Many targets, such as radome, sidewall of ship, shell launching port, air inlet of aircraft's engine and body of armored vehicle possess the cavity structures which would cause multiple reflections and alter the scattering characteristic of target. Numerical method is commonly utilized method to investigate the EM scattering of target. Taking the method of moment (MOM) [1] and the multilevel fast multipole algorithm (MLFMA) [2] as representative examples, they are impractical for calculating the electrically large-scale problems in realistic engineering field due to memory requirement constraints. The high-frequency method is very suitable for solving the electrically large-scale problems. For example, physical optics (PO) [3] is a representative one. However, when target possesses the cavity structure and the multiple reflections are dominant, PO is no longer applicable and accurate. In 1989, the shooting and bouncing ray (SBR) [4] was proposed by Ling *et al* to solve the scattering problems of open-ended cavities. The SBR has evolved into a standard method to calculate the scattering problems of object with cavity structure. This method describes the multiple bouncing in cavity structure by virtue of geometrical optics (GO) and PO approximation concepts, in which GO regulates the rules of the wave propagation and the PO integrations are implemented to obtain the scattering field. Its accuracy could be controlled by regulating ray density and number of reflections and transmissions, respectively. At first, the SBR was used to analyze EM scattering from objects with corner

The associate editor coordinating the review of this manuscript and approving it for publication was Wen-Sheng Zhao.

This work is licensed under a Creative Commons Attribution 4.0 License. For more information, see https://creativecommons.org/licenses/by/4.0/

structure [5]–[6]. Then, some scattering problems of actual targets with cracks, gaps or small protrusions were considered [7]–[9]. Zhang *et al.* [10] utilized the SBR to give the scattering simulation of radomes and dielectric lenses. Ding *et al.* [11] analyzed EM scattering of cavities with nonuniform plasma coating. Weinmann and Vauple [12] studied the scattering from a metallic cavity filled with dielectric material. Li *et al.* [13] proposed an improved SBR based on Unigraphics to calculate the RCS of cavity target. At the technical level, SBR has also been greatly improved. Ji *et al* proposed a method that uses triangular ray tubes [14] in place of the conventional rectangular tubes [15] to improve the efficiency and accuracy of SBR. Graphics processing unit (GPU)-based parallelization with compute unified device (CUDA) [16] was utilized to model the EM wave propagation from dielectrics and perfect conductors. Dong *et al.*[17] utilized OpenGL and neighbor search technique to accelerate the SBR and studied the EM scattering from complex objects. Guo and Guo [18] proposed the near field SBR based on PO near field integral to analyze the near field scattering problems.

These research achievements show the efficiency and diverse applications of SBR. Nevertheless, most of these achievements focus on the study of scattering from target with carved surface or cavity structure. A few researchers also have studied environmental scattering or scattering from target above relatively flat surface. However, there is a kind of environment with natural cavity structure existing in the nature, which is always simplified or neglected by researchers. The valley environment is the representative one. With the washing and erosion by waters, the valley environment contains the water surface and the mountain structure with cavity characteristics. This special structure makes its scattering mechanism more complicated. When target is located above valley environment, multiple interactions between target and natural cavity structure will have tremendous impact on target's scattering characteristic.

For this kind of environment, our research group has done several tentative works, e.g., the modeling for water zone embedded in land surface [19] and the adjacent region between ground and near sea [20]. In this paper, the geometrical model of valley environment is established referring to the theory of composite rough surface modeling [20]. Conventional SBR method could calculate the far field by opening surface integral according to the Huygens' principal. However, the valley composite rough surface has no tangible opening surface. Although the SBR with PO type integration does not need to compute the opening surface integral, it is also unable to obtain the field on every facet, even the surface currents. Therefore, the concept of ray-density normalization (RDN) [21] is introduced. It can be utilized to determine field of the facet which the ray passes through according to the relationship between the power of ray and the area of illuminated facet. In this paper, the SBR with RDN is applied to simulate the complex ray propagation in the valley's cavity structure and multiple interactions between low-latitude target and valley environment. The equivalent edge currents (EEC) [22] method is introduced to meliorate the results after ray propagation process which makes the final results more accurate.

The rest of paper is organized as following: In Section II, the formulations of SBR based on the RDN are described. The theory of EEC method is reviewed. Several examples are given to verify the validation of hybrid SBR-EEC method. In Section III, firstly, a low-altitude prismatic table above valley environment with different polarization mode is considered to discuss the influence of polarization mode on scattering characteristic; Secondly, a low-altitude cube above valley environments with diverse statistic parameters combination is considered to discuss the influence of roughness parameters on scattering characteristic; Finally, the EM scattering characteristics of low-altitude aircraft above valley environment are investigated. In Section IV, some discussion and conclusions are provided and a proposition for further research is given.

II. FORMULATION

A. THE SHOOTING AND BOUNCING RAY BASED ON RAY-DENSITY NORMALIZATION

We adopt the triangular facets to simulate the surface of low-altitude target and valley environment. Figure 1 shows the sketch map for geometrical structure of composite model and the process of ray propagation. The SBR technique describes multiple bouncing in cavity structure by GO and PO approximation concepts. The multiple bouncing between different triangular facets on model's surface is calculated by GO. At the last reflection position, the PO integration based on the induced surface currents is utilized to compute the far field of the ray tubes.

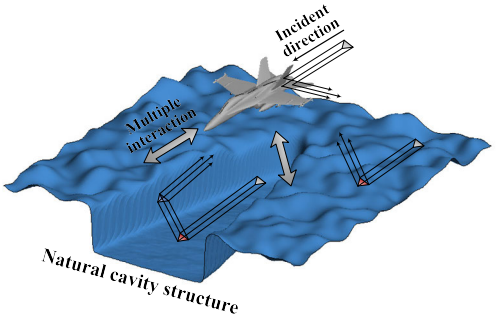

FIGURE 1. The sketch map for geometrical structure of composite model and the process of ray propagation.

The incident wave is plane wave and the expression of electric field (includes the time factor $e^{j\omega t}$) is taken in the form:

$$\mathbf{E}_i^0 = A_i^0 \hat{\mathbf{e}}_i^0 e^{j\phi_0} \tag{1}$$

where A_i^0 denotes initial electric field intensity; ϕ_0 denotes initial electric field phase; $\hat{\mathbf{e}}_i^0$ presents direction of polarization. θ_i and φ_i present incident pitch angle and incident

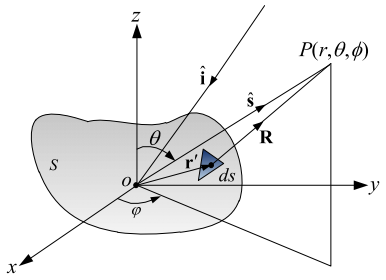

FIGURE 2. The sketch map of EM scattering from the triangle facet.

azimuth angle. Direction of polarization is presented as follow

$$\hat{\mathbf{e}}_i^0 = \begin{cases} (\cos\theta_i \cos\phi_i, \cos\theta_i \sin\phi_i, -\sin\theta_i), & \text{vertical polarization} \\ (-\sin\phi_i, \cos\phi_i, 0), & \text{horizontal polarization} \end{cases} \tag{2}$$

After determining the polarization mode and intensity of electric field, the initial incident electric field vector of each ray is determined. The relationship between incident vector and reflective vector obeys the Snell reflection theorem [6]. The reflection electric field $\mathbf{E'}_r(\mathbf{r}_{P_i})$ can be obtained from the incident electric field $\mathbf{E'}_i(\mathbf{r}_{P_i})$. Their relationships are given as follow:

$$\mathbf{E'}_i(\mathbf{r}_{P_i}) = \mathrm{E}_v\hat{\mathbf{e}}_v + \mathrm{E}_h\hat{\mathbf{e}}_h \tag{3a}$$
$$\mathbf{E'}_r(\mathbf{r}_{P_i}) = (DF)_i(\mathrm{R}_v\mathrm{E}_v\hat{\mathbf{e}}_v + \mathrm{R}_h\mathrm{E}_h\hat{\mathbf{e}}_h) \tag{3b}$$

where the subscript v and h present vertical polarization and horizontal polarization, respectively. $(DF)_i$ denotes the diffusion coefficient of facet S_n, and its detailed description is given in [23]. R_v and R_h present reflection coefficient in vertical polarization and horizontal polarization, respectively [4].

By virtue of GO theorem, the i-th reflection electric field can be calculated by the i-th incident electric field. Then, the i-th reflection electric field is used as the $(i+1)$-th incident electric field. The amplitude and phase tracking can be realized by such sequential calculation.

After the process of ray tracing, the far field of each ray is calculated by PO integral. The far field of triangle facet can be written as

$$\mathbf{E}^s \approx (jk/4\pi)(e^{-jkr}/r)\left[\hat{\mathbf{s}} \times (\mathbf{M}_s + \eta_0\hat{\mathbf{s}} \times \mathbf{J}_s)\right] \cdot \Delta A \cdot \mathrm{I} \tag{4}$$

where $\mathbf{J}_s$ and $\mathbf{M}_s$ denote electric current and magnetic current on the facet; If the facet belongs to PEC surface, the magnetic current $\mathbf{M}_s$ equals to $\mathbf{0}$; k denotes wave number: $k = 2\pi/\lambda$; ΔA denotes the area of triangle facet; I denotes the Fourier transform form of the triangle shape function, whose expression is given as follow:

$$\mathrm{I} = (1/\Delta A)\int_S \exp[jk\mathbf{r}' \cdot (\hat{\mathbf{s}} - \hat{\mathbf{i}})]ds' \tag{5}$$

The equation above satisfies the form of Gordon integral method [24], and it can be written as:

$$\mathrm{I} = \frac{1}{jk|\hat{\mathbf{n}} \times \mathbf{w}|\Delta A}\sum_{m=1}^{3}(\hat{\mathbf{n}} \times \mathbf{w}) \cdot \mathbf{a}_m \exp(jk\mathbf{r}_m \cdot \mathbf{w}) \sin c(\frac{1}{2}k\mathbf{a}_m \cdot \mathbf{w}) \tag{6}$$

where $\mathbf{w} = \hat{\mathbf{s}} - \hat{\mathbf{i}}$, $\sin c(x) = \sin x/x$; $\mathbf{a}_m$ denotes the length and the orientation of the m-th side of facet f_i; $\mathbf{r}_m$ is position vector of midpoint of the m-th side; $\hat{\mathbf{i}}$ and $\hat{\mathbf{s}}$ are unit vector of incident and scattering direction, respectively. When $|\hat{\mathbf{n}} \times \mathbf{w}| = 0$, the expression of I can be rewritten as:

$$\mathrm{I} = \exp(jk\mathbf{r}_0 \cdot \mathbf{w}) \tag{7}$$

where $\mathbf{r}_0$ denotes the position vector of arbitrary point in triangle facet f_i. In this paper, we choose the centroid of triangle as this point. Finally, far field of all facets are added, then the preliminary far field of the composite model is obtained. Based on the equivalence principle, the electric current $\mathbf{J}_s$ and magnetic current $\mathbf{M}_s$ on facet can be obtained by equation $\mathbf{J}_s = \hat{\mathbf{n}} \times \mathbf{H}_s$ and $\mathbf{M}_s = -\hat{\mathbf{n}} \times \mathbf{E}_s$. The $\mathbf{E}_s$ and $\mathbf{H}_s$ denote total electric field and total magnetic field, respectively. In the condition of PO approximation, they could be calculate by adding the incident field $\mathbf{E}_i$, $\mathbf{H}_i$ and the reflection field $\mathbf{E}_r$, $\mathbf{H}_r$ based on GO, which are taken in these forms:

$$\mathbf{E}(\mathbf{r}') = \mathbf{E}_i(\mathbf{r}') + \mathbf{E}_r(\mathbf{r}') \tag{8a}$$
$$\mathbf{H}(\mathbf{r}') = \mathbf{H}_i(\mathbf{r}') + \mathbf{H}_r(\mathbf{r}') \tag{8b}$$

The reflection field can be obtained by equation (3a) and (3b). However, there are multiple incident rays existing in one triangular facet. These rays will lead to multiple incident fields with different amplitude and direction of propagation. Thus, the RDN theory [21] is introduced. The core of RDN theory is to determine the field of the facet which the ray passes through according to the relationship between the power of ray and the area of illuminated facet [25]. As shown in Figure 3, assuming the emission surface is rectangular, the sides of the rectangle are $X_{\max}$ and $Y_{\max}$. They are disserted by n_{xn} and n_{yp} respectively. Thus, there will be $2n_{xn}n_{yp}$ triangles with same area.

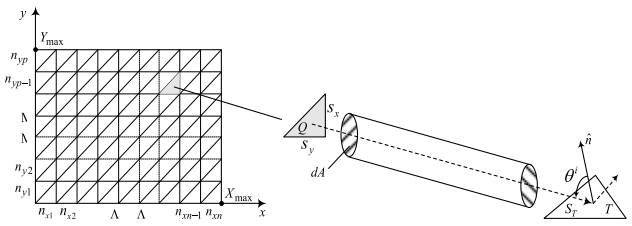

FIGURE 3. The definition and propagation process of single ray.

Take an arbitrary triangle Q as the emission surface of single ray, the ray density is defined as the number of rays in unit area, whose expression is shown as follow:

$$n_d = 2n_{xn}n_{yp}/X_{\max}Y_{\max} \tag{9}$$

Correspondingly, the area of each ray can be written as:

$$dA = 1/n_d = X_{\max} Y_{\max}/2n_{xn}n_{yp} \tag{10}$$

Assume the area of triangle is S_T, the number of rays in j-th incidence is taken in this form:

$$M_j = n_d^j S_T \cos\theta_i \tag{11}$$

$\mathbf{E}_t^i(r)$ and $\mathbf{H}_t^i(r)$ denote the total incident electric field and incident magnetic field [26] of a facet determined by ray tracing, which can be written as

$$\mathbf{E}_t^i(r) = \sum_{j=1}^{N_r} X_j^c \mathrm{E}_j(\hat{\mathbf{h}}_j \times \hat{\mathbf{k}}_j)\exp(-j\mathbf{k}_j \cdot \mathbf{r}_j) \tag{12a}$$

$$\mathbf{H}_t^i(r) = \sum_{j=1}^{N_r} X_j^c \mathrm{H}_j \hat{\mathbf{h}}_j \exp(-j\mathbf{k}_j \cdot \mathbf{r}_j) \tag{12b}$$

where N_r denotes the total times of reflection; E_j and H_j denote amplitude of electric field and magnetic field, respectively. There is a relationship $\mathrm{H}_j = \mathrm{E}_j/\eta_0$, where η_0 denotes wave impedance in free space; $\hat{\mathbf{h}}_j$ denotes direction of polarization; $\mathbf{k}_j$ denotes wave vector; and $\mathbf{r}_j$ denotes position vector of reflection point; X_j^c is amplitude weighted factor, which can be written as:

$$X_j^c = dA/S_T = 1/n_d^j \cos(\theta_j^i) S_T \tag{13}$$

B. EQUIVALENT EDGE CURRENTS METHOD

In scattering computation process, the scattering caused by the edge structure may always be neglected. However, this kind of structure commonly exists in the actual flying target. In 1980s, Michaeii has verified the effect of edge structure on the scattering characteristics and proposed the EEC method [22] to compute it. In this paper, EEC is utilized to consider the edge diffraction from the low-altitude target. The contribution of edge structure will be added into total field to enhance the accuracy of the final numerical results. The edge diffraction is obtained by substituting the equivalent electric/magnetic current into the radiation integral.

As shown in Figure 4, the far field of edge diffraction is obtained by the integral on edge C, whose expression is shown as follow:

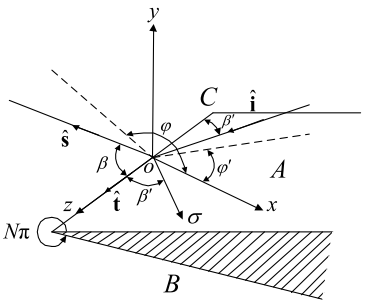

FIGURE 4. The sketch map of wedge construction.

$$\mathbf{E}^d = \frac{jk}{4\pi}\frac{e^{-jkr}}{r}\int_C \{Z_0\hat{\mathbf{s}} \times [\hat{\mathbf{s}} \times \mathbf{J}(\mathbf{r}')] + \hat{\mathbf{s}} \times \mathbf{M}(\mathbf{r}')\} e^{jk\hat{\mathbf{s}}\cdot\mathbf{r}'} dl \tag{14}$$

where Z_0 denotes the wave impedance in free space; $\mathbf{J}(\mathbf{r}') = \mathrm{I}_e(\mathbf{r}')\hat{\mathbf{t}}$ and $\mathbf{M}(\mathbf{r}') = \mathrm{I}_m(\mathbf{r}')\hat{\mathbf{t}}$ denote equivalent electric current and equivalent magnetic current of edge C, respectively; $\hat{\mathbf{t}}$ denotes unit tangential vector of edge C; $\hat{\mathbf{s}}$ denotes unit vector of observation direction; $\mathbf{r}'$ denotes vector from original point to a point located in edge C; dl is arc length increment of edge C; $N\pi$ denotes exterior angle of wedge. $\mathrm{I}_e(\mathbf{r}')$ and $\mathrm{I}_m(\mathbf{r}')$ are taken in the forms:

$$\mathrm{I}_e(\mathbf{r}') = \mathrm{I}_T^A + \mathrm{I}_T^B \tag{15a}$$

$$\mathrm{I}_m(\mathbf{r}') = \mathrm{M}_T^A + \mathrm{M}_T^B \tag{15b}$$

where the superscripts A and B present the contributions from wedge face A and face B, which are shown in Figure 4. The subscript T presents the truncated term. The truncated term could be obtained by the untruncated term and the correction term, which are represented by subscripts U and C respectively. $\mathrm{I}_e(\mathbf{r}')$ and $\mathrm{I}_m(\mathbf{r}')$ can be written as:

$$\mathrm{I}_e(\mathbf{r}') = (\mathrm{I}_U^A - \mathrm{I}_C^A) + (\mathrm{I}_U^B - \mathrm{I}_C^B) \tag{16a}$$

$$\mathrm{I}_m(\mathbf{r}') = (\mathrm{M}_U^A - \mathrm{M}_C^A) + (\mathrm{M}_U^B - \mathrm{M}_C^B) \tag{16b}$$

Detailed descriptions of the untruncated term and the correction term of both electric current and magnetic current can refer to [27]. By virtue of the treatment for singularities [28], the EEC method can be safely and efficiently used to compute te edge diffraction at all directions of incidence and observation.

III. NUMERICALSIMULATION AND DISCUSSION

A. MODELING OF VALLEY COMPOSITE ROUGH SURFACE

The valley environments are characterized by cavity, compositionality and complexity. The valley circumstance contains both ground surface and water surface, which is obviously shown in Figure 5.

FIGURE 5. The actual valley environments.

In this subsection, we assume that the statistic properties of valley environment's water surface obey the PM spectral distribution. The PM spectrum [29] is taken in this form:

$$W_{PM}(k) = \frac{\alpha_p}{2k^3}\exp(-\frac{\beta g^2}{v_{19.5}^4 k^2}) \tag{17}$$

where α_p and β denote dimensionless empirical constants: $\alpha_p = 8.1 \times 10^{-3}$, $\beta = 0.74$; g_c denotes gravity acceleration, $g_c = 9.81\text{m/s}^2$; In rectangular coordinate system, k can be presented as $k^2 = k_x^2 + k_y^2$; $v_{19.5}$ denotes wind velocity on the height of 19.5m above sea surface, which controls the roughness of the sea surface. It is just an approximate method to model the water surface. It is feasible to use some more suitable spectral functions. Correspondingly, we adopt Gaussian spectral function [30] to simulate the ground surface of valley environment, whose expression is taken in this form:

$$W\left(k_x, k_y\right) = \frac{l_x l_y h_{\text{rms}}^2}{4\pi} \exp\left(-\frac{k_x^2 l_x^2}{4} - \frac{k_y^2 l_y^2}{4}\right) \tag{18}$$

where h_{rms} denotes root mean square (RMS) height; l_x and l_y denote correlation lengths along x-axis and y-axis, respectively. Both of them belong to a kind of tentative approach. If the prospecting data for the valley environment's surface profile distribution can be obtained, it will make the modeling more practical.

At first, we give the review of the modeling method for composite rough surface from [20]. The most important procedure in modeling process is the filtering processing by weighted inverse tangent function, which is taken in this form:

$$\begin{aligned} f_{com}(x, y) = & f_{sur1}(x, y) \cdot [\pi/2 + \arctan f_w(x, y)]/\pi \\ & + f_{sur2}(x, y) \cdot [\pi/2 - \arctan f_w(x, y)]/\pi \end{aligned} \tag{19}$$

where $f_{sur1}(x, y)$, $f_{sur2}(x, y)$ and $f_{com}(x, y)$ present the profile distribution of rough surface region $sur1$, rough surface region $sur2$ and composite rough surface com respectively; $f_w(x, y)$ denotes the weighted function for simulating the shape of borderline, whose concrete form depends on the actual structure of environment. The sketch map of the composite rough surface modeling is shown in Figure 6.

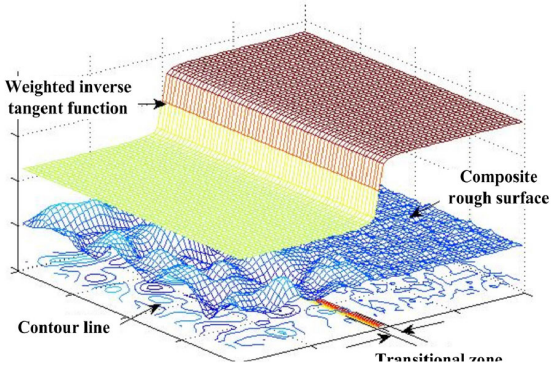

FIGURE 6. The sketch map of composite rough surface modeling.

The statistic properties of ground region are determined by parameters of Gaussian spectrum [30], e.g., RMS height h_{rms} and correlation lengths along x-axis and y-axis l_x, l_y. The surface characteristic of water surface is controlled by parameters of PM spectrum [29], e.g., the wind velocity on the height of 19.5 m above sea surface $v_{19.5}$. Here, we review the weighted inverse tangent function for valley environment [29], whose expression is shown as follow:

$$\begin{aligned} & f_{valley}(x, y) = w_1 \cdot [f_{gro}(x, y) + H_{gro}] + w_2 \cdot f_{sea}(x, y) \\ & \begin{cases} w_1 = [\pi/2\text{-arctan}(ax + bL_x - y^2)]/\pi \\ w_2 = [\pi/2\text{+arctan}(ax + bL_x - y^2)]/\pi \end{cases} \end{aligned} \tag{20}$$

where $f_{gro}(x, y)$, $f_{sea}(x, y)$ and $f_{valley}(x, y)$ present the surface profile distribution of ground rough surface, sea surface and valley composite rough surface, respectively; w_1 and w_2 present the weighted factors; H_{gro} denotes the depth factor which controls the depth of valley; L_x denotes the length of total surface along x-axis direction; a and b present the width factor and length factor which are used for changing the opening width and valley length of the valley composite rough surface. The working frequency is set as 300 MHz; Size of environment is $L_\text{x} \times L_\text{y}$: 40m × 40m; The shape parameters of valley are set as: $\text{H}_{gro} = 5.0$, $a = 2.0$ and $b = 0.5$; The RMS is set as $h_{\text{rms}} = 0.5\lambda$ and the correlation lengths along x-axis and y-axis direction are set as $l_x = l_y = 2.0\lambda$; The wind velocity on the height of 19.5 m above sea surface is set as $v_{19.5} = 0.3\text{m/s}$. The simulation result of valley environment is shown in Figure 7.

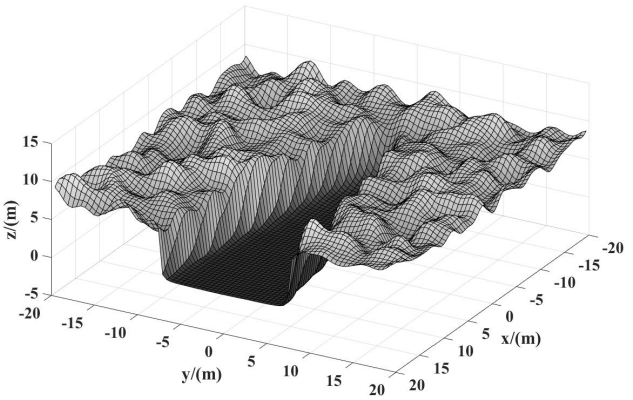

FIGURE 7. The simulation result of valley environment.

In Figure 7, the valley composite rough surface comprises the obvious cavity structure. In actual natural environment, the borderline between the ground region and water region should be non-linear and more complex. We can also use different forms of weighted inverse tangent function to realize more complicated borderline that we need.

B. VERIFICATION OF HYBRID SBR-EEC METHOD

In this subsection, we consider two computation examples to verify the efficiency and accuracy of hybrid SBR-EEC method. We choose three algorithms as the reference algorithm, e.g., the conventional MOM with bi-conjugate gradient method (Bi-CGM), SBR with RDN and conventional PO. In this paper, when we apply the SBR, up to ten reflections are included, which ensures the accuracy and sufficient convergence of the results [21]. First, the example of a PEC

dihedral reflector above Gauss rough surface is considered. Working frequency is set as 300 MHz; Size of environment is $L_x \times L_y$: 40m × 40m. The dihedral reflector is composed of two squares with side length of 6.0m and its height above rough surface is set as 5.0m. Eight sampling points are considered per wave length. The Gauss rough surface is set as PEC surface and its statistic parameters are: $h_{\rm rms} = 0.1\lambda$, $l_x = l_y = 2.0\lambda$. The incident angles are set as $\theta_i = 45°$ and $\varphi_i = 0°$. The observation angle ranges from θ_s = -90° to $\theta_s = 90°$; Polarization mode is vertical-to-vertical (VV) polarization. The numerical results are obtained based on one surface realization. The scattering coefficient in this paper denotes radar cross section, which is represented as ''dBsm'' in the following figures. In this paper, the computing platform is AMD processor of 2.3 GHz with 64 kernels and 64 GB RAM.

Figure 8 shows the bi-static scattering coefficient (BSC) of a dihedral reflector above Gauss rough surface by hybrid SBR-EEC method and above three reference algorithms. As we see, there is a strong peak value existing in the specular scattering direction, because of the contribution from the relatively flat rough surface. In the backscattering region, there is also an obvious peak value due to the contribution from the dihedral structure. The BSC curves computed by MOM and SBR-EEC are in good agreements. Comparing the BSC curves obtained by SBR-EEC and SBR, we can find out that EEC method provides melioration at some scattering angles. But the effects are not obvious because of the little amounts of edge structure. We utilize the average deviation and maximum deviation to analyze the difference of the numerical results, whose expressions are taken into the forms:

$$\langle\gamma\rangle = \frac{1}{N_{\theta_s}} \sum_{\{\theta_s\}} \left|\gamma^{\rm T}(\theta_s) - \gamma^{\rm Rer}(\theta_s)\right| \tag{21a}$$

$$\max\gamma = \max_{\{\theta_s\}} \left|\gamma^{\rm T}(\theta_s) - \gamma^{Rer}(\theta_s)\right| \tag{21b}$$

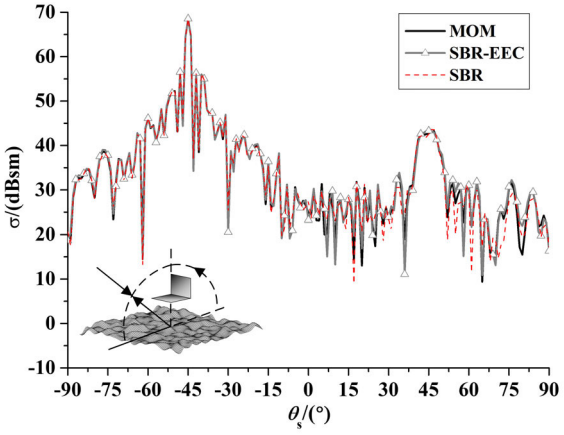

FIGURE 8. The simulation results of dihedral reflector above Gauss rough surface by different algorithms.

The average deviation and maximum deviation between MOM and SBR are 1.4721 dB and 8.3241 dB. The average deviation and maximum deviation between MOM and SBR-EEC are 0.9627 dB and 2.8318 dB. As we see, both of their average deviation is small, but the maximum deviation between MOM and SBR is too large. The introduction of EEC improves the accuracy of SBR. The consuming time of MOM is 5.76 h, and the consuming time of SBR-EEC is 0.98 h. The efficiency and accuracy of hybrid SBR-EEC method is verified.

To give the further validation of hybrid SBR-EEC method, we consider a PEC pyramid above valley composite rough surface. The working frequency and size of environment are the same as previous example. The pyramid is composed by four equilateral triangles with the side length of 6.0 m and its height above valley environment is set as 5.0 m. The position of pyramid is shown in Figure 9. The shape parameters of valley are set as: $H_{gro} = 5.0$, $a = 2.0$ and $b = 0.5$; The statistic parameters of valley are set as: $h_{\rm rms} = 0.1\lambda$, $l_x = l_y = 2.0\lambda$ and $v_{19.5} = 0.3$m/s. Relative permittivity of ground region equals to 10.95-j8.73 when soil's humidity is 20 %, soil density is 20.0 %, sand density is 54.5 %, which is obtained based on the semi-empirical formulas proposed in [31]; Relative permittivity of sea region equals to 71.37-j324.47 when water's salinity equals to 40 %, temperature is 20 °C, which is obtained based on the Debye expression [31]. The incident angles are set as $\theta_i = 45°$ and $\varphi_i = 0°$. The observation angle ranges from $\theta_s = -90°$ to $\theta_s = 90°$; Polarization mode is VV polarization.

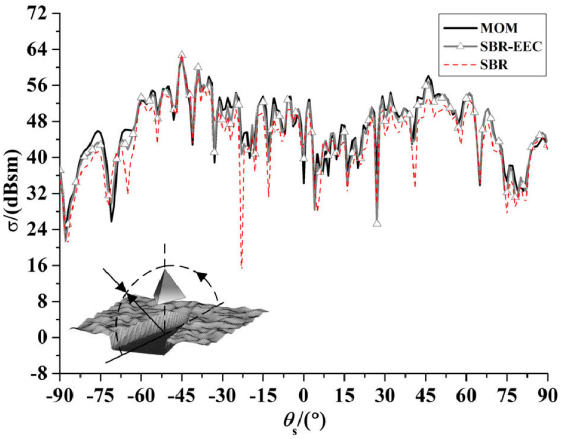

FIGURE 9. The simulation results of pyramid above valley composite rough surface by different algorithms.

Figure 9 shows the BSC of a pyramid above valley composite rough surface by hybrid SBR-EEC method and above three reference algorithms. As we see, the scattering energy is concentrated in the region of specular scattering and backscattering. The peak value in the specular scattering direction is no longer obvious. The total scattering energy distributing near the backscattering region increases apparently due to the cavity structure of valley environment and the multiple interaction between pyramid and rough surface.

The BSC curves computed by MOM and SBR-EEC are in good agreements. Comparing with the results of Figure 8, the effect of EEC to meliorate target's edge diffraction is obvious because the pyramid has a certain number of edges. The average deviation and maximum deviation between MOM and SBR are 3.5796 dB and 27.3469 dB. The average deviation and maximum deviation between MOM and SBR-EEC are 0.8415 dB and 2.9384 dB. As we see, both the average deviation and the maximum deviation between MOM and SBR is too large. The introduction of EEC improves the accuracy of SBR. The consuming time of MOM is 7.63 h, and the consuming time of SBR-EEC is 1.24 h. Therefore, the above numerical results verify that hybrid SBR-EEC method is an efficient tool to solve the scattering problems of target above valley environment.

C. A PRISMATIC TABLE MODEL ABOVE VALLEY COMPOSITE ROUGH SURFACE WITH DIFFERENT POLARIZATION MODE

To investigate the influence of polarization mode on the scattering characteristics of a simple object above valley environment, we consider a PEC prismatic table model above the valley rough surface. Working frequency is set as 300 MHz. The size and shape parameters of valley environment are the same as previous example, and the relative permittivities of each region are the same as previous example. The bottom side length and top side length are 8.0 m and 4.0 m, respectively, and its height is set as 4.0 m. The height above rough surface is set as 5.0 m. The following numerical simulations obtained by hybrid SBR-EEC method are determined by averaging 30 Monte Carlo realizations. The incident angles are set as $\theta_i = 45°$ and $\varphi_i = 0°$. The observation angle ranges from $\theta_s = -90°$ to $\theta_s = 90°$; The VV polarization, vertical-to-horizontal (VH) polarization, horizontal-to-vertical (HV) polarization and horizontal-to- horizontal (HH) are considered. The BSC curves of a PEC prismatic table above valley composite rough surface with different polarization mode are given in Figure 10.

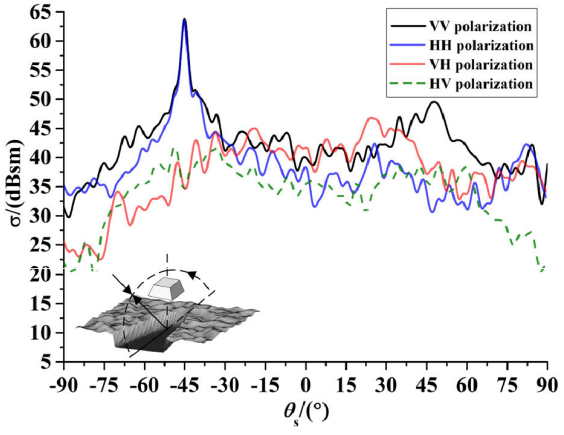

FIGURE 10. The BSC curves of a PEC prismatic table above valley composite rough surface with different polarization mode.

In Figure 10, the curve of VV polarization presents strong specular peak value and obvious backscattering. In the curve of HH polarization, there is also a strong peak value at the direction of specular scattering, but the backscattering is no longer obvious. The curves of both VH and HV polarization presents no obvious regular characteristic. In terms of scattering coefficient, the curve values of VH polarization are larger than that of HV polarization in the scattering angle range from $-38°$ to $42°$ and $60°$ to $90°$. In the scattering angle range from $-68°$ to $-47°$, the curve values of HV polarization are larger than that of VH polarization.

D. A CUBE MODEL ABOVE VALLEY COMPOSITE ROUGH SURFACE

To investigate the scattering characteristics of a simple object above valley environment, we consider a PEC cube above the valley rough surface. Simultaneously, the effects of valley environment's statistic parameters on the EM scattering are discussed. Working frequency is set as 300 MHz. The size and shape parameters of valley environment are the same as previous example, and the relative permittivities of each region are the same as previous example. The cube's side length and its height above rough surface are set as 5.0 m. The valley environments with four kinds of statistic parameters combination are considered, which are shown in the legend of Figure 11. The incident angles are set as $\theta_i = 45°$ and $\varphi_i = 0°$. The observation angle ranges from $\theta_s = -90°$ to $\theta_s = 90°$; Polarization mode is set as VV polarization. The BSC curves of a PEC cube above valley composite rough surface with different statistic parameters combination of valley composite rough surface are given in Figure 11.

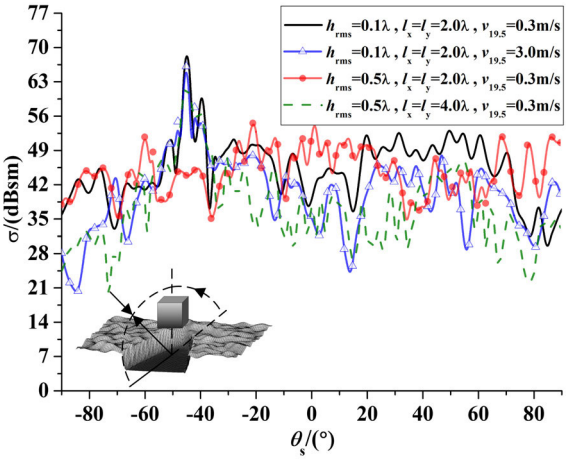

FIGURE 11. The BSC curves of a PEC cube above valley composite rough surface with different statistic parameters combination.

In Figure 11, when a cube is located above the first kind of valley environment, except for the peak value at the specular direction ($\theta_s = -45°$), there is also a peak value existing at the scattering angle of -40°. The cavity structure of valley leads to the splitting of specular scattering energy. There is also a wide range of backscattering region existing in the scattering

angle range from 17° to 66°, which is caused by the target and the multiple interactions between target and valley's cavity structure. In the second kind of valley environment, when the water surface becomes rougher, the peak value at specular direction decreases, and the scattering energy at almost scattering angles declines at some degrees. In the third kind of valley environment, when the ground surface becomes rougher, the total curve presents a strong diffuse scattering characteristic. In the fourth kind of valley environment, with the increase of correlation length, the correlation of every point in surface enhances. Though the RMS is large, the total roughness will become relatively smaller. Thus, there is also a peak value existing at the specular direction, but the value is smaller than the first two cases. Although the larger correlation length makes the peak value appear again, but the total roughness is still very large, which leads to the weak scattering energy at the other scatting angles. Compared with the first case, the backscattering of the last three cases is significantly weaker. The reason causes this phenomenon is that the relatively rougher surface will weaken the interaction effect between the target and environmental surface, even though the cavity structure exists.

E. AN AIRCRAFT MODEL ABOVE VALLEY COMPOSITE ROUGH SURFACE

In this computation example, the influence of valley environment on the scattering characteristic of a low-altitude aircraft target is analyzed. Working frequency is set as 300 MHz. Size of environment is $L_x \times L_y$: 60m × 60m. The shape parameters of valley are set as: $H_{gro} = 10.0$, $a = 2.0$ and $b = 0.5$; The relative permittivity settings are the same as previous. The aircraft model is set as PEC. The fuselage length, wingspan length and fuselage height are 17.5 m, 12.1 m and 3.6 m, respectively. We consider the mono-static scattering of the front incidence ($\theta_i = -90° \sim 90°$ and $\varphi_i = 0°$) and the side incidence ($\theta_i = -90° \sim 90°$ and $\varphi_i = 90°$), and the concrete sketch maps of the position relationship between incidence wave and scattering model are given in Figure 12. The mono-static scattering coefficient curves of an aircraft model above valley composite rough surface with different incidence direction are calculated by using the hybrid SBR-EEC method, which are given in Figure 12.

As shown in Figure 12(a), the mono-static scattering of an aircraft model is unevenly distributed in the space. The mono-static scattering in the angle range of −15° to 15° is relatively stronger compared to other angles due to the contribution of flat wing surfaces and fuselage. There are also some strong scattering region existing in the space, which mainly comes from the protruding fuselage and tailpipes. The scattering near the nose cone direction is relatively smaller than other angles due to the stealth design of the aircraft. When the aircraft model is located above valley composite rough surface, the existence of valley's cavity structure leads to the multiple interactions between target and cavity, which will make the scattering characteristic more complicated and enhance the scattering intensity at most scattering angles.

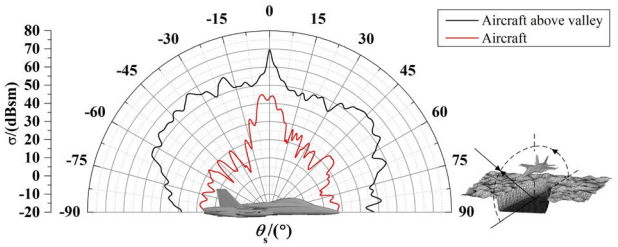

(a) The mono-static scattering coefficient of the front incidence.

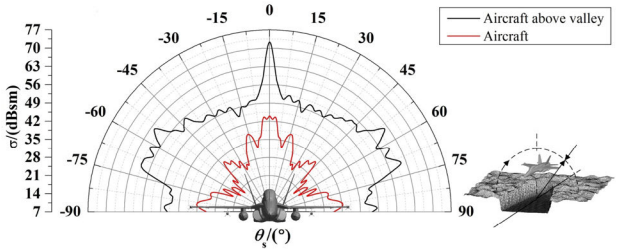

(b) The mono-static scattering coefficient of the side incidence.

FIGURE 12. The mono-static scattering coefficient curves of an aircraft model above valley composite rough surface with different incidence direction.

As shown in Figure 12(b), the mono-static scattering of an aircraft model is symmetrically distributed in the space because of the symmetrical shape of aircraft.

In Figure 12(b), in the scattering angle region 0° to 90°, there are four obvious peak values at the scattering angle 0°, 15°, 44°, and 87°, respectively. The fuselage, wings, ailerons and tails comprise several quasi-dihedral structures which will bring strong backscattering. The curve in another half of the angle region presents the same characteristic. When the aircraft model is located above valley composite rough surface, the existence of valley's cavity structure also has tremendous impact on scattering characteristic of the target. Through many realizations and average processing, the mono-static scattering coefficient curve of composite model also presents symmetry. There is an obvious peak value at the scattering angle of 0°, which mainly comes from the scattering of rough surface and flat wing surfaces. In the scattering angle region 0° to 90°, there is a strong scattering region existing in the angle region from 53° to 70°. The first reason causes this phenomenon is that the quasi-dihedral structure comprised of fuselage and wing surface could bring strong backscattering. The second reason is that the side surface of valley's mountain and the water surface also form the quasi-dihedral structure which could enhance the scattering intensity. The third reason is that the multiple interactions between target and cavity structure may change the scattering energy distribution at some degree. The curve in another half of the angle region presents the same characteristic.

IV. CONCLUSION

In this paper, a hybrid SBR-EEC method is proposed to study the EM scattering characteristics of low-altitude target above valley environment. The theory for modeling of composite rough surface is reviewed and the modeling method for valley

environment with cavity structure is given. The formulations and basic theory of the hybrid SBR-EEC method is presented and some numerical examples are provided to verify the validation of this hybrid algorithm. The numerical results show a conclusion that the contribution of edge diffraction is obvious only when the target has obvious edge structure. A composite scattering model of a prismatic table above valley environment is considered, and the influence of polarization mode on its scattering characteristic are discussed in detail. A composite scattering model of a cube above valley environment is considered, and the influences of RMS, correlation length and wind velocity on its scattering characteristic are discussed in detail. A low-altitude aircraft target is considered, and the scattering characteristics of it above valley environment are investigated. Consequently, the proposed hybrid SBR-EEC method can be used as an efficient tool to investigate the EM scattering characteristics of low-latitude target above the valley environment with cavity structure. And the valley's cavity structure will tremendously alter the scattering intensity distribution of low-altitude target which will has influence on the detection for target located above the valley environment. The further works of our research group will focus on two directions: firstly, more detailed modeling method should be studied. The surface of each region in valley environment could be generated by different spectrum, such as exponential spectrum. And the detailed components such as rocks, plants, or sands, etc. will make the environmental model more practical. Secondly, the scattering problems about the combined target like the coated objects or combined conducting and dielectric objects above this valley environment, in order to find out more valuable phenomena and useful conclusions.

REFERENCES

[1] S. Rao, D. Wilton, and A. Glisson, "Electromagnetic scattering by surfaces of arbitrary shape," *IEEE Trans. Antennas Propag.*, vol. 30, no. 3, pp. 409–418, May 1982.
[2] J. M. Song and W. C. Chew, "Multilevel fast-multipole algorithm for solving combined field integral equations of electromagnetic scattering," *Microw. Opt. Technol. Lett.*, vol. 10, no. 1, pp. 14–19, Sep. 1995.
[3] S. W. Lee, J. Baldauf, H. Ling, and R. Chou, "Twelve versions of physical optics: How do they compare?" in *IEEE AP-S Symp. Dig. Syracuse*, New York, NY, USA, Jun. 1988, pp. 408–411.
[4] H. Ling, R.-C. Chou, and S.-W. Lee, "Shooting and bouncing rays: Calculating the RCS of an arbitrarily shaped cavity," *IEEE Trans. Antennas Propag.*, vol. 37, no. 2, pp. 194–205, Feb. 1989.
[5] J. Baldauf, S.-W. Lee, L. Lin, S.-K. Jeng, S. M. Scarborough, and C. L. Yu, "High frequency scattering from trihedral corner reflectors and other benchmark targets: SBR versus experiment," *IEEE Trans. Antennas Propag.*, vol. 39, no. 9, pp. 1345–1351, Sep. 1991.
[6] H. Kim and H. Ling, "Electromagnetic scattering from an inhomogeneous object by ray tracing," *IEEE Trans. Antennas Propag.*, vol. 40, no. 5, pp. 517–525, May 1992.
[7] J. M. Jin, S. Ni, and S. W. Lee, "Robust hybrid technique for calculating scattering by large and complex targets," *Electron. Lett.*, vol. 30, no. 25, pp. 2169–2170, Dec. 1994.
[8] J.-M. Jin, S. S. Ni, and S.-W. Lee, "Hybridization of SBR and FEM for scattering by large bodies with cracks and cavities," *IEEE Trans. Antennas Propag.*, vol. 43, no. 10, pp. 1130–1139, Oct. 1995.
[9] J.-M. Jin, F. Ling, S. T. Carolan, J. M. Song, W. C. Gibson, W. C. Chew, C.-C. Lu, and R. Kipp, "A hybrid SBR/MoM technique for analysis of scattering from small protrusions on a large conducting body," *IEEE Trans. Antennas Propag.*, vol. 46, no. 9, pp. 1349–1357, Sep. 1998.
[10] Y. Zhang, J. Wang, Z. Zhao, and J. Yang, "Numerical analysis of dielectric lens antennas using a ray-tracing method and HFSS software," *IEEE Antennas Propag. Mag.*, vol. 50, no. 4, pp. 94–101, Aug. 2008.
[11] J. Ding, S. Shang, R. Chen, and Z. H. Fan, "Analysis of electromagnetic scattering of cavities with nonuniform plasma coating," in *Proc. IEEE Int. Conf. Microw. Millim. Wave Technol.*, May 2010, pp. 148–151.
[12] F. Weinmann and T. Vaupel, "SBR simulations and measurements for cavities filled with dielectric material," in *Proc. IEEE Antennas Propag. Soc. Int. Symp.*, Jul. 2010, pp. 1–4.
[13] J. Z. Li, X. Y. Wang, and W. Z. Wang, "A new shooting and bouncing rays algorithm based on unigraphics and its application in cavity targets," *IEEE Int. Appl. Comput. Electromagn. Soc. Symp.*, Sep. 2017, pp. 1–2.
[14] J. Ji, J. Liu, and Y. Ma, "Triangular ray tubes in electromagnetic scattering calculation using shooting and bouncing ray (SBR)," *Optik*, vol. 127, no. 5, pp. 3117–3120, Mar. 2016.
[15] S. Suk, T.-I. Seo, H.-S. Park, and H.-T. Kim, "Multiresolution grid algorithm in the SBR and its application to the RCS calculation," *Microw. Opt. Technol. Lett.*, vol. 29, no. 6, pp. 394–397, 2001.
[16] R. Brem and T. F. Eibert, "A shooting and bouncing ray (SBR) modeling framework involving dielectrics and perfect conductors," *IEEE Trans. Antennas Propag.*, vol. 63, no. 8, pp. 3599–3609, Aug. 2015.
[17] C.-L. Dong, L.-X. Guo, X. Meng, and Y. Wang, "An accelerated SBR for EM scattering from the electrically large complex objects," *IEEE Antennas Wireless Propag. Lett.*, vol. 17, no. 12, pp. 2294–2298, Dec. 2018.
[18] G. Guo and L. Guo, "SBR method for near-field scattering of an electrically large complex target illuminated by dipole sources," *IEEE Access*, vol. 6, pp. 78710–78718, 2018.
[19] H. L. Sun, C. M. Tong, and G. X. Zou, "High efficiency iterative solver for modeling composite rough surface electromagnetic scattering," *Electromagnetics*, vol. 37, no. 2, pp. 113–126, Mar. 2017.
[20] G. X. Zou, C. M. Tong, H. L. Sun, T. Wang, and P. Peng, "A hybrid method for electromagnetic scattering from target above composite rough surface of ground and near sea in adjacent region," *Electromagnetics*, vol. 38, no. 7, pp. 415–437, Jan. 2018.
[21] D. Didascalou, T. M. Schafer, F. Weinmann, and W. Wiesbeck, "Ray-density normalization for ray-optical wave propagation modeling in arbitrarily shaped tunnels," *IEEE Trans. Antennas Propag.*, vol. 48, no. 9, pp. 1316–1325, Sep. 2000.
[22] A. Michaeli, "Equivalent edge currents for arbitrary aspects of observation," *IEEE Trans. Antennas Propag.*, vol. 32, no. 3, pp. 252–258, Mar. 1984.
[23] M. G. Wang, *Theory of Geometric Diffraction*, 2nd ed. Xi'an, China: Xidian Univ. Press, 1994.
[24] W. B. Gordon, "High frequency approximations to the physical optics scattering integral," *IEEE Trans. Antennas Propag.*, vol. 42, no. 3, pp. 427–432, Mar. 1994.
[25] F. Z. Geng, S. R. Peng, K. B. Qin, Y. F. Pan, and H. W. Sun, "An MOM-SBR/PO hybrid method for scattering by complex objects," *Chin. J. Comput. Phys.*, vol. 27, no. 2, pp. 269–273, 2010.
[26] F. Weinmann, "Ray tracing with PO/PTD for RCS modeling of large complex objects," *IEEE Trans. Antennas Propag.*, vol. 54, no. 6, pp. 1797–1806, Jun. 2006.
[27] P. M. Johansen, "Uniform physical theory of diffraction equivalent edge currents for truncated wedge strips," *IEEE Trans. Antennas Propag.*, vol. 44, no. 7, pp. 989–995, Jul. 1996.
[28] A. Hujanen and J. E. Sten, "Study of scattering by a perfectly conducting wedge with finite sized faces," *Annales des Telecommun.*, vol. 56, nos. 9–10, pp. 587–594, 2001.
[29] G.-X. Zou, C.-M. Tong, W.-M. Liu, B. Chen, and G.-H. Wu, "Research on electromagnetic scattering characteristics of strait composite random rough surface based on improved hybrid SBR/PO method," in *Proc. 11th Int. Symp. Antennas, Propag. EM Theory (ISAPE)*, Oct. 2016, pp. 587–591.
[30] G. Brown, "Backscattering from a Gaussian-distributed perfectly conducting rough surface," *IEEE Trans. Antennas Propag.*, vol. AP-26, no. 3, pp. 472–482, May 1978.
[31] M. Hallikainen, F. Ulaby, M. Dobson, M. El-Rayes, and L.-K. Wu, "Microwave dielectric behavior of wet soil—Part 1: Empirical models and experimental observations," *IEEE Trans. Geosci. Remote Sens.*, vol. GE-23, no. 1, pp. 25–34, Jan. 1985.

GAOXIANG ZOU was born in Hunan, China, in 1993. He received the B.S. degree in radar engineering and the M.S. degree in electronics science and technology from Air Force Engineering University, Xi'an, China, in 2015 and 2018, respectively, where he is currently pursuing the Ph.D. degree in electromagnetic theory and engineering.

His research interests include computational electromagnetism, Brewster effect, multipath effect, modeling theory of divisional environments and electromagnetic scattering characteristics of composite targets above divisional environments.

CHUANGMING TONG was born in Hubei, China, in 1964. He received the M.S. and Ph.D. degrees in electromagnetic field and microwave technology from Air Force Missile College, in 1988 and 1999, respectively. From 1999 to 2002, he was a Visiting Scholar with the State Key Laboratory of Millimeter Waves, Southeast University, Nanjing, China. He is currently a Professor and Doctoral Supervisor with Air and Missile Defense College, Air Force Engineering University. He is currently the Chief Scientist of National 973 project. His research interests include microwave remote sensing, computational electromagnetism, polarimetric and interferometric applications of microwave data, and numerical modeling, ground penetrating radar, through wall imaging and stealth technology. He has received various fellowships and awards from national and international bodies.

JIAN ZHU was born in Jiangsu, China, in 1983. He received the B.S. degree in measurement, control technology and instrumentation from the Nanjing Institute of Technology, Nanjing, China, in 2006, and the M.S. degree in signal and information processing from the University of Science and Technology, Nanjing, in 2008. He is currently a Senior Engineer. He is working with the Shanghai Radio Equipment Research Institute. He is currently the Head of the subproject belonging to the National 973 project.

His research interests include the design of radar system design, radar missile signal processing, MIMO array signal processing, anti-jamming algorithms, target detection and tracking.

HUALONG SUN was born in Shaanxi, China, in 1982. He received the B.S. degree in information engineering from the Nanjing University of Aeronautics and Astronautics, Nanjing, China, in 2004, the M.S. degree in electromagnetic field and microwave technology from Southeast University, Nanjing, in 2007, and the Ph.D. degree in electromagnetic theory and engineering from Air and Missile Defense College, Air Force Engineering University, Xi'an, China, in 2017. He is currently a Postdoctoral student in electronics science and technology with Air and Missile Defense College, Air Force Engineering University.

His research interests include multipath effect, radar signal processing, fast electromagnetic calculation method, and electromagnetic scattering characteristics of complex targets and complicated circumstances.

PENG PENG was born in Jiangxi, China, in 1990. He received the B.S. degree in radar engineering and the M.S. degree in electromagnetic field and microwave technology from Air force Engineering University, in 2011 and 2013, respectively. From 2014 to 2015, he took the Initial Officer Training Course (IOTC) in the Royal Air force College Cranwell, U.K. He is currently pursuing the Ph.D. degree with the School of Physics and Optoelectronic Engineering, Xidian University, Xi'an, China.

His research interests include fast algorithms for computational electromagnetics, radar scattering characteristics of the complex target and environment surface, and radar imaging.